UCLA
UCLA Previously Published Works

Title

Corrigendum to "The influence of magnetic fields in planetary dynamo models" [Earth Planet. Sci. Lett. 333–334 (2012) 9–20]

Permalink

https://escholarship.org/uc/item/08t8k3vp

Authors

Soderlund, KM
King, EM
Aurnou, JM

Publication Date

2014-04-01

DOI

10.1016/j.epsl.2014.01.052

Peer reviewed

Corrigendum

Corrigendum to "The influence of magnetic fields in planetary dynamo models" [Earth Planet. Sci. Lett. 333–334 (2012) 9–20]

K.M. Soderlund [a,*], E.M. King [b], J.M. Aurnou [c]

[a] *Institute for Geophysics, Jackson School of Geosciences, University of Texas at Austin, Austin, TX 78758, USA*
[b] *Department of Earth and Planetary Science, University of California, Berkeley, CA 94720, USA*
[c] *Department of Earth, Planetary, and Space Sciences, University of California, Los Angeles, CA 90095, USA*

A R T I C L E   I N F O

We have investigated the influence of magnetic fields on the convective properties of planetary dynamo models and the transition between dynamos with dipolar and multipolar magnetic fields in Soderlund et al. (2012). We thank Uli Christensen for pointing out an error solely in our algorithm used to calculate the volumetric average of relative axial helicity, H_z^{rel}. However, it should be noted that the main results of the paper remain intact, as discussed below.

Relative axial helicity is defined as axial helicity normalized by its maximum possible value,

$$H_z^{rel} = \frac{\langle u_z \omega_z \rangle_h}{(\langle u_z u_z \rangle_h \langle \omega_z \omega_z \rangle_h)^{1/2}}, \tag{1}$$

where u_z is axial velocity, $\omega_z = \nabla \times \mathbf{u} \cdot \hat{\mathbf{z}}$ is axial vorticity, and $\langle \rangle_h$ is the volumetric average in each hemisphere excluding boundary layers (e.g., Olson et al., 1999; Schmitz and Tilgner, 2010). We average the helicity magnitude over each hemisphere since axial helicity tends to be anti-symmetric across the equator and assume Ekman boundary layer thicknesses of $\delta_E/D = 3E^{1/2}$ following King et al. (2012).

In Soderlund et al. (2012), the $|H_z^{rel}|$ calculations are missing a factor of $\sin\theta$ in the volume integral. The erroneously calculated helicity data are shown in Fig. 1a. The effect of this missing factor is to weight the contributions within the tangent cylinder too heavily.

Corrected $|H_z^{rel}|$ are shown in Fig. 1b. While instantaneous values were given in Soderlund et al. (2012), here we report the average of three random snapshots in time for each case. Temporal

standard deviations (σ) are typically near 0.02. The corrected values differ on average from the original values by [0.02 (0.02), 0.04 (0.04), 0.07 (0.02)] for cases with $E = [10^{-3}, 10^{-4}, 10^{-5}]$ where parentheses indicate non-magnetic cases. These differences only exceed 2σ in the lowest Ekman number dynamo cases.

Tables 1 and 2 provide corrected values of $|H_z^{rel}|$. In addition, we have also included time averaged values of axial vorticity columnarity $C_{\omega z}$, in situ Lorentz to Coriolis force ratio F_L/F_C, and in situ inertial to viscous force ratio F_I/F_V.

The two main conclusions of the paper are not modified significantly. They are: (i) The magnetic fields do not strongly affect relative axial helicity in cases with $E \geqslant 10^{-4}$. This weak influence can be understood theoretically by estimating the strength of the Lorentz forces in the high magnetic Reynolds number limit with a dynamic Elsasser number, $\Lambda_d = B^2/(2\rho\mu_o \Omega U \ell_B)$. Calculations of the dynamic Elsasser number correctly capture the secondary influence of Lorentz forces on convection. (ii) The breakdown of dipolar magnetic field generation still coincides with the degradation of helicity in the flow, even though the helicity decreases are markedly less abrupt than originally reported (see Fig. 1b). Importantly, the dipolarity breakdown still occurs when the inertial and viscous forces become comparable, $F_I/F_V \sim 1$, for all Ekman numbers considered here ($10^{-3} \geqslant E \geqslant 10^{-5}$). Because viscosity is expected to be negligible in planetary settings, the dipolarity breakdown in present day dynamo models with moderate Ekman numbers may not extrapolate to planets.

DOI of original article: http://dx.doi.org/10.1016/j.epsl.2012.03.038.

* Corresponding author. Tel.: +1 (218) 349 3006; fax: +1 (512) 471 8844.
E-mail addresses: krista@ig.utexas.edu (K.M. Soderlund), eric.king@berkeley.edu (E.M. King), aurnou@ucla.edu (J.M. Aurnou).
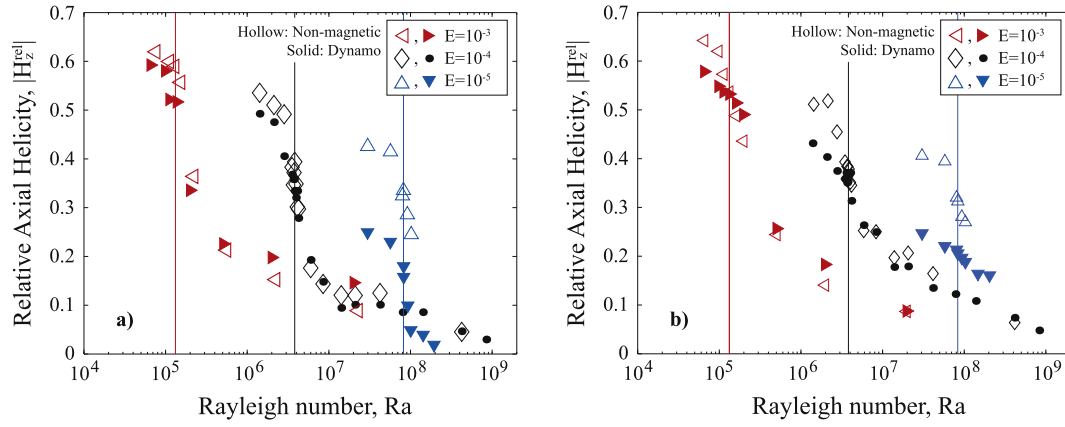
Fig. 1. (a) Instantaneous relative axial helicity, $|H_z^{rel}|$, versus the Rayleigh number published in Soderlund et al. (2012). (b) Corrected relative axial helicity, $|H_z^{rel}|$, versus the Rayleigh number using the average of three random snapshots in time. The temporal standard deviations are typically ~0.02; errorbars are not included for clarity. Vertical lines denote the transition between dipolar and multipolar dynamos (at $f = 0.5$). Filled (hollow) markers denote dynamo (non-magnetic) models.

Table 1
Input and time-averaged output parameters for fixed $\chi = 0.4$, $Pr = 1$, $Pm = 2$, and $E = 10^{-4}$. Non-magnetic values are given in parentheses. The average of three random snapshots in time are used to calculate $C_{\omega z}$, $|H_z^{rel}|$, F_L/F_C, and F_I/F_V; single snapshots were used in Soderlund et al. (2012). All parameters are defined in Tables 1 and 2 of Soderlund et al. (2012). Asterisks indicate the use of hyperdiffusion.

Ra	$\frac{Ra}{Ra_c}$	N_{ro}	l_{max}	Nu	Re_c	Re	$C_{\omega z}$	$|H_z^{rel}|$	$\bar{k}_u$	$\bar{k}_B$	f	Λ_i	Λ_d	λ	$\frac{F_L}{F_C}$	$\frac{F_I}{F_V}$
1.42×10^6	1.9	41	64	1.88	33	34	0.70	0.43	15.0	11.6	0.89	1.30	0.14	0.06	0.18	0.44
				(1.74)	(41)	(43)	(0.70)	(0.51)	(17.4)							(0.67)
2.12×10^6	2.8	41	64	2.55	51	52	0.63	0.40	17.2	13.6	0.76	2.10	0.17	0.09	0.21	0.68
				(2.32)	(64)	(67)	(0.63)	(0.52)	(19.6)							(0.94)
2.83×10^6	3.8	41	64	3.19	70	72	0.57	0.38	18.6	15.8	0.65	2.42	0.17	0.11	0.24	0.83
				(2.98)	(89)	(92)	(0.62)	(0.46)	(19.4)							(1.25)
3.54×10^6	4.7	41	64	3.78	89	91	0.55	0.36	19.5	18.0	0.57	2.37	0.15	0.12	0.27	1.01
				(3.74)	(113)	(118)	(0.60)	(0.39)	(18.9)							(1.62)
3.68×10^6	4.9	41	64	3.88	93	95	0.56	0.37	19.6	18.6	0.56	2.36	0.15	0.13	0.21	1.04
				(3.88)	(117)	(123)	(0.60)	(0.36)	(18.8)							(1.56)
3.75×10^6	5.0	41	64	3.94	96	98	0.58	0.35	19.7	18.9	0.55	2.27	0.14	0.13	0.21	1.11
				(3.94)	(119)	(125)	(0.59)	(0.38)	(18.8)							(1.60)
3.82×10^6	5.1	41	64	4.04	120	124	0.58	0.35	18.9	26.7	0.18	0.14	0.01	0.05	0.01	1.50
				(4.00)	(121)	(127)	(0.59)	(0.38)	(18.8)							(1.63)
3.96×10^6	5.3	41	64	4.15	123	128	0.59	0.37	19.0	26.6	0.16	0.18	0.01	0.05	0.02	1.56
				(4.13)	(126)	(132)	(0.59)	(0.38)	(18.7)							(1.67)
4.11×10^6	5.5	41	64	4.28	127	131	0.57	0.37	19.0	26.8	0.17	0.22	0.01	0.06	0.02	1.61
				(4.26)	(130)	(136)	(0.58)	(0.35)	(18.6)							(1.72)
4.24×10^6	5.6	41	85	4.38	130	135	0.59	0.31	19.0	27.1	0.20	0.24	0.02	0.06	0.02	1.60
				(4.36)	(133)	(140)	(0.57)	(0.35)	(18.6)							(1.75)
6.00×10^6	8.0	41	85	5.57	169	174	0.54	0.26	19.1	29.0	0.12	0.68	0.04	0.11	0.06	1.96
				(5.57)	(179)	(188)	(0.55)	(0.25)	(18.0)							(2.15)
8.50×10^6	11	41	128	6.72	210	216	0.50	0.25	19.0	31.4	0.12	1.53	0.07	0.17	0.11	2.27
				(6.77)	(231)	(246)	(0.49)	(0.25)	(17.7)							(2.79)
1.42×10^7	19	49	128	8.41	285	293	0.43	0.18	18.7	34.6	0.06	3.44	0.13	0.29	0.21	2.76
				(8.53)	(326)	(353)	(0.43)	(0.20)	(17.2)							(3.37)
2.10×10^7	28	49	128	9.73	357	368	0.37	0.18	18.6	37.8	0.06	5.48	0.18	0.40	0.28	3.09
				(9.91)	(417)	(453)	(0.36)	(0.21)	(17.0)							(4.26)
$2.10 \times 10^{7*}$	28	49	128	9.70	350	358	0.43	0.17	15.5	22.7	0.08	7.61	0.15	0.28	0.25	3.81
4.24×10^7	56	49	192	12.4	540	557	0.28	0.14	17.3	44.9	0.04	11.4	0.29	0.68	0.44	4.21
				(12.7)	(647)	(684)	(0.28)	(0.17)	(17.4)							(5.70)
8.00×10^7	106	49	192	15.1	820	845	0.24	0.12	15.6	51.0	0.03	20.7	0.40	1.05	0.59	5.38
1.42×10^8	188	65	192	17.8	1117	1153	0.22	0.11	14.5	58.0	0.04	36.3	0.58	1.57	0.81	6.65
$4.24 \times 10^{8*}$	562	65	192	23.4	1802	2017	0.19	0.07	12.5	50.5	0.05	106	0.84	2.34	1.18	11.8
				(24.9)	(2139)	(2472)	(0.18)	(0.06)	(13.7)							(16.9)
$8.48 \times 10^{8*}$	1125	65	192	27.0	2281	2613	0.18	0.05	13.2	46.3	0.02	197	1.11	2.92	1.63	16.3

Table 2

Input and time-averaged output parameters for fixed $\chi = 0.4$ and $Pr = 1$ using the notation of Table 1. Two dynamos with $E = 10^{-3}$ were found to decay with additional runtime.

Ra	$\frac{Ra}{Ra_c}$	N_{ro}	l_{max}	Nu	Re_c	Re	$C_{\omega z}$	$|H_z^{rel}|$	$\overline{k_u}$	$\overline{k_B}$	f	Λ_i	Λ_d	λ	$\frac{F_L}{F_C}$	$\frac{F_I}{F_V}$
$E = 10^{-3}$, $Pm = 5$																
6.50×10^4	1.9	37	42	1.45	10	10	0.76	0.58	7.1	7.9	0.78	4.34	0.42	0.15	0.39	0.33
				(1.43)	(13)	(13)	(0.75)	(0.64)	(9.7)							(0.39)
9.70×10^4	2.8	37	42	1.60	14	15	0.69	0.55	8.5	8.9	0.65	3.91	0.30	0.16	0.43	0.40
				(1.71)	(19)	(20)	(0.71)	(0.62)	(10.6)							(0.57)
1.12×10^5	3.2	37	42	1.80	19	20	0.70	0.54	8.6	9.7	0.54	3.25	0.20	0.16	0.40	0.48
				(1.82)	(22)	(23)	(0.71)	(0.57)	(10.6)							(0.64)
1.32×10^5	3.8	37	42	2.02	27	27	0.71	0.53	9.4	11.8	0.31	0.61	0.03	0.08	0.05	0.75
				(1.97)	(26)	(27)	(0.70)	(0.54)	(9.8)							(0.73)
1.60×10^5	4.6	37	42	2.16	31	31	0.68	0.51	9.7	–	–	$\to 0$	$\to 0$	$\to 0$	$\to 0$	0.90
				(2.16)	(31)	(32)	(0.66)	(0.49)	(9.8)							(0.84)
1.96×10^5	5.6	37	42	2.38	36	37	0.64	0.49	9.9	–	–	$\to 0$	$\to 0$	$\to 0$	$\to 0$	0.95
				(2.40)	(36)	(37)	(0.63)	(0.44)	(9.9)							(0.92)
5.00×10^5	14	37	64	3.55	69	70	0.52	0.26	9.4	19.6	0.14	4.14	0.15	0.36	0.29	1.39
				(3.59)	(74)	(75)	(0.49)	(0.24)	(9.5)							(1.72)
1.96×10^6	56	37	64	5.45	143	151	0.38	0.18	9.6	26.3	0.07	23.0	0.51	1.13	0.79	2.22
				(5.60)	(163)	(176)	(0.34)	(0.14)	(9.3)							(3.16)
1.96×10^7	560	37	64	10.7	419	454	0.23	0.09	12.7	37.7	0.02	248	2.62	5.35	4.20	3.68
				(11.3)	(526)	(565)	(0.21)	(0.09)	(13.1)							(5.54)
$E = 10^{-5}$, $Pm = 2$																
3.10×10^7	1.9	49	128	3.07	75	78	0.48	0.25	23.1	15.2	0.79	4.84	0.30	0.05	0.39	0.42
				(2.08)	(122)	(127)	(0.66)	(0.41)	(34.9)							(0.99)
5.89×10^7	3.6	49	170	5.09	153	159	0.42	0.22	29.7	22.0	0.58	7.07	0.31	0.08	0.45	0.71
				(4.01)	(271)	(284)	(0.60)	(0.39)	(33.9)							(1.95)
8.20×10^7	5.0	49	192	6.73	218	225	0.42	0.21	33.2	27.0	0.48	8.28	0.32	0.11	0.45	0.97
				(6.15)	(407)	(436)	(0.58)	(0.32)	(30.5)							(2.76)
8.50×10^7	5.2	49	192	6.81	224	231	0.40	0.19	32.9	27.4	0.47	8.54	0.32	0.11	0.47	0.96
				(6.45)	(420)	(454)	(0.57)	(0.31)	(30.5)							(2.89)
9.50×10^7	5.8	49	192	7.41	251	259	0.41	0.20	34.1	29.2	0.45	9.02	0.32	0.12	0.45	1.12
				(7.29)	(474)	(512)	(0.56)	(0.28)	(29.6)							(3.26)
1.05×10^8	6.5	49	192	8.03	274	283	0.40	0.19	35.5	30.7	0.42	9.63	0.33	0.14	0.47	1.17
				(8.17)	(524)	(570)	(0.55)	(0.27)	(29.2)							(3.59)
1.50×10^8	9.2	65	213	9.98	363	374	0.37	0.16	35.9	34.2	0.37	12.4	0.36	0.17	0.52	1.49
$2.00 \times 10^{8*}$	12.3	65	213	12.3	470	483	0.36	0.16	37.1	39.0	0.29	14.8	0.38	0.21	0.56	1.83

References

King, E.M., Stellmach, S., Aurnou, J.M., 2012. Heat transfer by rapidly rotating Rayleigh–Bénard convection. J. Fluid Mech. 691, 568–582.

Olson, P.L., Christensen, U.R., Glatzmaier, G.A., 1999. Numerical modeling of the geo- dynamo: Mechanisms of field generation and equilibration. J. Geophys. Res. 104, 10383–10404.

Schmitz, S., Tilgner, A., 2010. Transitions in turbulent rotating Rayleigh–Bènard con- vection. Geophys. Astrophys. Fluid Dyn. 104, 481–489.

Soderlund, K.M., King, E.M., Aurnou, J.M., 2012. The influence of magnetic fields in planetary dynamo models. Earth Planet. Sci. Lett. 333–334, 9–20.